JOURNAL OF SOLID STATE CHEMISTRY **127,** 222–230 (1996)
ARTICLE NO. 0378

Electron Diffraction Study of Interstitial Transition Metal Ordering in $T_{2+x}Sn_2$ (T = Co, Ni) $B8$-Type Solid Solutions

A-K. Larsson, R. L. Withers,[1] and L. Stenberg*

*Research School of Chemistry, Australian National University, Canberra, ACT, 0200, Australia; and *Inorganic Chemistry 2, Chemical Centre, Lund University, PO Box 124, S-221 00, Lund, Sweden*

Received January 30, 1996; in revised form September 9, 1996; accepted September 10, 1996

Interstitial transition metal ordering in the "disordered," wide-range nonstoichiometric $Ni_{2+x}Sn_2$, $0.70 < x < 1.19$, and $Co_{2+x}Sn_2$, $0.76 < x < 1.26$, solid solution fields has been investigated via electron and X-ray powder diffraction. The sublattice is of the NiAs type with additional interstitial transition metal ions occupying trigonal bipyramidal sites in the Sn sub-lattice. That the distribution of interstitial sites is far from random in these "disordered" phases is clear from the presence of a spectacular and highly structured diffuse intensity distribution which appears to take the form of undulating, approximately cylindrical channels of diffuse intensity running along the c* direction of reciprocal space. The strongest satellite reflections of a low-temperature superstructure phase in each system are shown to fall more or less directly onto the diffuse distribution of the "disordered" phase. The characteristic extinction conditions of the superstructure phase are mirrored in the characteristic shape of the diffuse distribution of the "disordered" phase. The composition dependence of the diffuse distribution is investigated.

1. INTRODUCTION

Wide-range nonstoichiometric solid solutions intermediate in composition between the $B8_1$ NiAs structure type and the $B8_2$ Ni_2In structure type occur quite commonly in T–B systems (1–3), T being a transition metal and B a chalcogenide, pnictide, or element from the boron or carbon group. In such systems, the main group metal, B, forms an essentially hexagonal close-packed (hcp) array into the octahedral and trigonal bipyramidal interstices of which are located the T_1 and T_2 transition metal atoms. The T_1, or octahedral, sites are always fully occupied, whereas the trigonal bipyramidal, or T_2, sites are usually only partially occupied, giving rise to overall stoichiometry $T_{2+x}B_2$. The fully occupied T_1B array is of the NiAs type. The underlying average structure space group symmetry of such systems is hexagonal $P6_3/mmc$ ($a \approx 4$ Å, $c/a \approx 1.2$–1.3) with B in Wyckoff position $2c\ \frac{1}{3}\ \frac{2}{3}\ \frac{1}{4}$, the octahedrally coordinated T_1 in position $2a$ 000, and the partially occupied T_2 in Wyckoff position $2d\ \frac{1}{3}\ \frac{2}{3}\ \frac{3}{4}$ (see Fig. 1).

With slow cooling from the temperature of synthesis (typically ~ 900–1100 K) to room temperature, ordering of the occupied and vacant interstitial T_2 sites occurs, giving rise to a diverse array of long-range ordered superstructure phases (4, 5). To obtain a well-ordered superstructure phase, it is often also necessary to anneal for several days at 600–700 K (6). The detection and characterization of such ordered superstructure phases are difficult since the cell parameters of the underlying average structure typically remain metrically very close to hexagonal and multiple twinning on a reasonably fine scale is common (7). Furthermore, the additional superlattice reflections arising from the T_2 metal atom ordering and associated structural relaxation are often rather weak and difficult to detect with standard X-ray methods. On heating of these ordered superstructures to somewhat higher temperatures, there is usually a weakly first-order phase transition to a disordered NiAs–Ni_2In-type state (6). Alternatively, this so-called disordered NiAs–Ni_2In-type phase can be obtained by cooling more rapidly from the higher temperatures of synthesis.

As a result of the sudden disappearance of the sharp satellite reflections characteristic of the lower-temperature interstitial T_2 site ordering at the order–disorder phase transition (6), it is usually presumed that the occupied interstitial T_2 sites become randomly distributed in this higher-temperature disordered phase. There are, however, a whole range of degrees of order intermediate between long-range order and complete disorder in such wide-range nonstoichiometric systems (8–14).

This paper focuses on the $Co_{2+x}Sn_2$ and $Ni_{2+x}Sn_2$ systems (6, 15). The low-temperature γ' forms of $Co_{2+x}Sn_2$ and $Ni_{2+x}Sn_2$ ($2x + 1 \sim 3$) are reported to be isostructural. In the setting of Ref. (7), the orthorhombic space group is $Pnma$ ($\mathbf{a}_0 = \mathbf{a}_h - \mathbf{b}_h$, $\mathbf{b}_0 = -\mathbf{c}_h$, $\mathbf{c}_0 = 2\mathbf{a}_h + 2\mathbf{b}_h$) and its reciprocal lattice ($\mathbf{a}_0^* = \frac{1}{2}(\mathbf{a}_h^* - \mathbf{b}_h^*) = -\mathbf{b}_h^* + \frac{1}{2}(\mathbf{a}_h^* + \mathbf{b}_h^*)$, $\mathbf{b}_0^* = -\mathbf{c}_h^*$, $\mathbf{c}_0^* = \frac{1}{4}[\mathbf{a}_h^* + \mathbf{b}_h^*]$) is characterized by the

[1] To whom all correspondence should be addressed.

0022-4596/96 $18.00

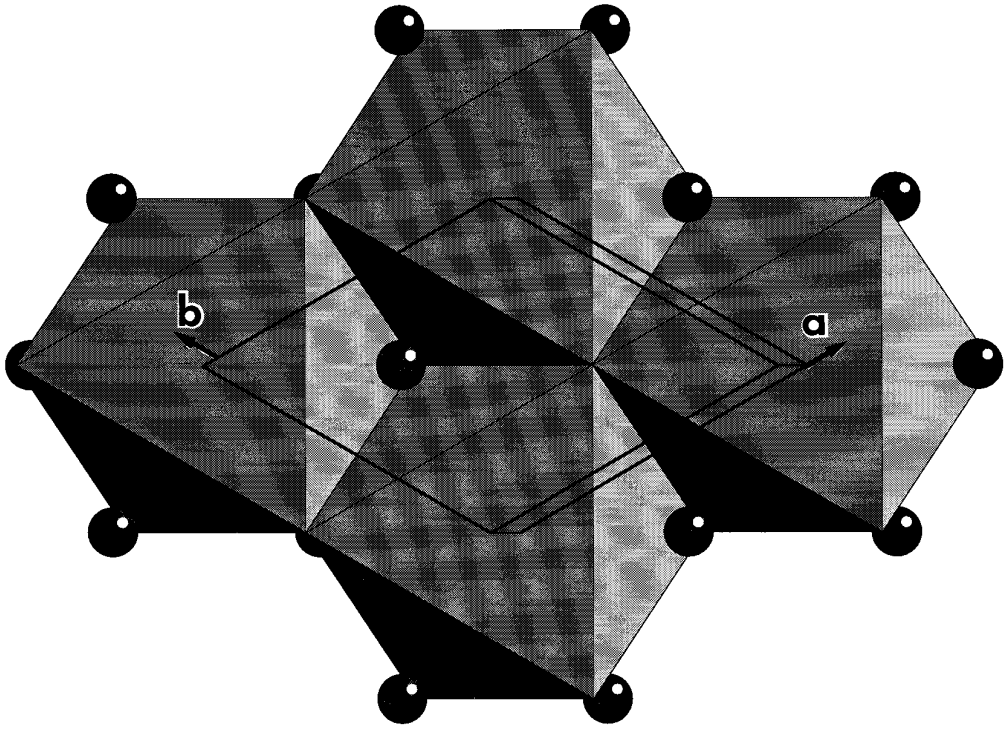

FIG. 1. Ideal "disordered" parent $(T)_{2+x}B_2$ structure projected slightly away from [001]. Only atoms with z fractional coordinates between $\frac{1}{4}$ and $\frac{3}{4}$ are shown. The T_1B NiAs-type octahedral array is shown along with the partially occupied, interstitial T_2 sites (shown as spheres). Note the $\langle 110 \rangle$ strings of interstitial T_2 sites. The average structure until cell is outlined and the unit cell axes marked. Note that there are two interstitial T_2 sites per parent unit cell ($M3$ and $M4$) related by a c glide perpendicular to $[\bar{1}10]$ in the average structure.

existence of sharp additional satellite reflections at $\mathbf{G}_h + n\mathbf{q}$, where $\mathbf{G}_h$ refers to the strong Bragg reflections of the underlying $P6_3/mmc$ average structure, and $\mathbf{q}$, the primary modulation wavevector (16) characteristic of the occupational interstitial T_2 site ordering, is given by $\frac{1}{4}(\mathbf{a}_h^* + \mathbf{b}_h^*)$. The real space distribution of atoms in γ'-$Ni_{2+x}Sn_2$ was first solved by Brand (17) and confirmed for γ'-$Co_{2+x}Sn_2$ by Rajeswari and Manihar (18). The interstitial T_2 atoms form zigzag chains along $\mathbf{a}_0$ at $\mathbf{b}_0 = \frac{1}{4}$ and $\frac{3}{4}$ [see Fig. 1 of (7)]. Fjellvåg and Kjekshus (6) found the homogeneity range of existence of this γ' phase in the $Ni_{2+x}Sn_2$ system to be $Ni_{2.7}Sn_2$ to $Ni_{3.1}Sn_2$, whereas in the $Co_{2+x}Sn_2$ system, single-phase γ' was found only with the composition $Co_{2.9}Sn_2$. Note that partial occupancies are implied whenever x does not equal 1.

According to both Fjellvåg and Kjekshus (6) and Ellner (15), the homogeneity range of existence of the disordered phase (at 1000–1050 K and in specimens quenched to room temperature from these temperatures) extends from $Co_{2.76}Sn_2$–$Co_{3.26}Sn_2$ in the case of the $Co_{2+x}Sn_2$ system (i.e., from 38 to 63% occupancy of the interstitial T_2 site) and from $Ni_{2.70}Sn_2$–$Ni_{3.19}Sn_2$ (i.e., from 35 to 60% occupancy of the interstitial T_2 site) in the case of the $Ni_{2+x}Sn_2$ system. The relatively large structural relaxations associated with occupancy of a particular T_2 site (4, 17, 18) suggest that there must exist strong local rules governing the arrangement of the occupied sites. The purpose of this paper is to investigate via electron diffraction the nature of this interstitial T_2 atom ordering in the disordered phase and its relationship to the lower-temperature long-range ordered superstructure phase.

2. EXPERIMENTAL

Synthesis

Samples of $Ni_{2+x}Sn_2$ of varying composition were prepared by mixing together Ni powder (4N, Koch–Light Laboratories Ltd.) reduced by H_2 at 550°C and Sn (99.999%) granules in appropriate ratios, pressing into pellets, sealing under vacuum in silica tubes, and heating at 900°C for 3 days. The product was then quenched in water. A part of this sample was annealed for a further 10 days at 700°C followed by quenching in water. Samples of $Co_{2+x}Sn_2$ of varying composition were similarly prepared by mixing together Co powder (4N, Koch–Light Laboratories Ltd.) reduced by H_2 at 550°C and Sn (99.999%) granules in appropriate ratios, pressing into pellets, sealing under vacuum in silica tubes, and heating at 1000°C for 3 days. The samples were then quenched in air. A further sample of nominal composition $Co_{2.5}Sn_2$ (Co sponge, 5N Halewood

Chemicals Ltd., reduced under H_2 at 550°C, and Sn, 99.999%, granules) was pressed into pellets, arc melted, crushed, sealed in evacuated silica tubes, and heated at 1150°C for 3 months followed by quenching in water.

Characterization

Specimens were examined by XRD using a Guinier–Hägg camera with monochromated Cu$K\alpha_1$ radiation. For the determination of unit cell dimensions, an internal standard of Si (NBS No. 640) was added to calibrate the measurement of XRD films. Specimens for electron microscopy were prepared by crushing and dispersing onto holey-carbon-coated copper grids. These grids were then examined in JEOL 2000FX, JEOL 100CX, and Philips EM430 transmission electron microscopes.

3. RESULTS

That the distribution of occupied interstitial sites in the quenched, high-temperature (or disordered) phase is far from random was immediately apparent from the highly structured diffuse intensity distribution characteristic of it (see Fig. 2). There was never any evidence of broken hexagonal symmetry as far as this diffuse distribution was concerned, and hence here, and in what follows, all reflections have been indexed with respect to the underlying $P6_3/mmc$ average structure. Even though the local symmetry of the superstructure phase is orthorhombic *Pnma*, hexagonal twinning occurs on quite a fine scale so that most experimentally obtained diffraction patterns are contributed to by all three orientation variants [see, e.g., Fig. 2b]. The diffraction patterns of the superstructure phase have been indexed with respect to the underlying $P6_3/mmc$ average structure in Fig. 2 so that the relationship between the disordered phase and the long-range ordered phase is apparent. (In what follows the subscript h is dropped and it is understood that all nonsubscripted real or reciprocal space directions, axes, etc., are defined with respect to the underlying $P6_3/mmc$ hexagonal average structure.)

Diffuse Intensity Distribution Characteristic of the Disordered Phase and Its Relationship to the Low-Temperature, Long-Range Ordered Phase

The quenched, high-temperature (or "disordered") phase exhibits a fascinating and rather characteristic diffuse intensity distribution to which the orthorhombic, long-range ordered superstructure phase is clearly closely related. Figure 2, for example, shows (a) [001], (c) [110], and (e) [441] zone axis diffraction patterns typical of the disordered phases of both $Co_{2+x}Sn_2$ and $Ni_{2+x}Sn_2$. Figures 2b, d, and f show corresponding diffraction patterns of the low-temperature, ordered superstructure phase. Note that the strongest satellite reflections of the superstructure phase [at $\mathbf{G} \pm \frac{1}{4}(\mathbf{a}^* + \mathbf{b}^*)$] in (b), (d), and (f) fall more or less directly onto the diffuse distribution in (a), (c), and (e) and that the diffuse distribution appears to peak strongly in the vicinity of the $\mathbf{G} \pm \frac{1}{4}(\mathbf{a}^* + \mathbf{b}^*)$ regions of reciprocal space (this is particularly apparent in Figs. 2a and e; the fact that there is usually continuous diffuse intensity linking the various $\mathbf{G} \pm \frac{1}{4}(\mathbf{a}^* + \mathbf{b}^*)$ regions of reciprocal space (see Figs. 2c and e) suggests that the diffuse distribution must be concentrated along well-defined surfaces in reciprocal space. It is important, however, to point out that the relative intensity of the diffuse on these surfaces varies strongly with position on the surface, as is clear, for example, from Fig. 2e.

Note also the very clear "size effect" transfer of intensity from the high- to the low-angle side (19) of the $(h\mathbf{a}^* + k\mathbf{b}^*) \cdot \frac{1}{3}[-\mathbf{a} + \mathbf{b}] = \frac{1}{3}(-h + k) =$ an integer lines of reciprocal space in Fig. 2a (compare, e.g., the relative intensity of the closely spaced pairs of apparent superlattice reflections on either side of such a line arrowed in Fig. 2a). This effect is most visible toward the edge of the pattern where the redistribution of intensity due to multiple scattering is less pronounced. Note further that the characteristic extinction conditions of the *Pnma* superstructure phase are mirrored in the diffuse distribution of the "disordered" phase. The n glide perpendicular to $\mathbf{a}_0$ $(= \mathbf{a} - \mathbf{b})$ of the orthorhombic superstructure phase, for example, requires that $\mathbf{G} \pm \frac{1}{4}(\mathbf{a}^* + \mathbf{b}^*)$-type satellite reflections occur only around the c glide forbidden $\mathbf{G} = h(\mathbf{a}^* + \mathbf{b}^*) + l\mathbf{c}^*$, l odd, parent structure reflections as shown in Fig. 2d. The characteristic sine wave-type diffuse streaking along the $\mathbf{c}^*$ direction of Fig. 2c similarly only passes through $\mathbf{G} \pm \frac{1}{4}(\mathbf{a}^* + \mathbf{b}^*)$ regions of reciprocal space for $\mathbf{G} = h(\mathbf{a}^* + \mathbf{b}^*) + l\mathbf{c}^*$, l odd; i.e., not only do the sharp satellite reflections of the superstructure phase exhibit a characteristic extinction condition at this zone axis but so also does the diffuse intensity distribution characteristic of the disordered phase (8).

While the strongest satellite reflections of the superstructure phase fall more or less directly onto the diffuse distribution, note that the weaker second harmonic satellite reflections [at $\mathbf{G} \pm 2 \cdot \frac{1}{4}(\mathbf{a}^* + \mathbf{b}^*)$ in Figs. 2b and d] do *not* fall onto the diffuse distribution as is clear from Figs. 2a and c. This absence of the second harmonic satellite reflections is an absolutely characteristic signature of the "disordered" phase. The significance of the diffuse distribution is that it is giving a direct reciprocal space map of potential (i.e., low cost in terms of energy) compositional ordering patterns. The relative sharpness of the undulating sine wave-type scattering of Fig. 2c, for example, suggests that compositional ordering can only be associated with a remarkably selective range of modulation wavevectors. The reason for this is not at all clear. One possibility is that it may be related to some sort of electron counting rule as for the so-called Hume–Rothery alloys.

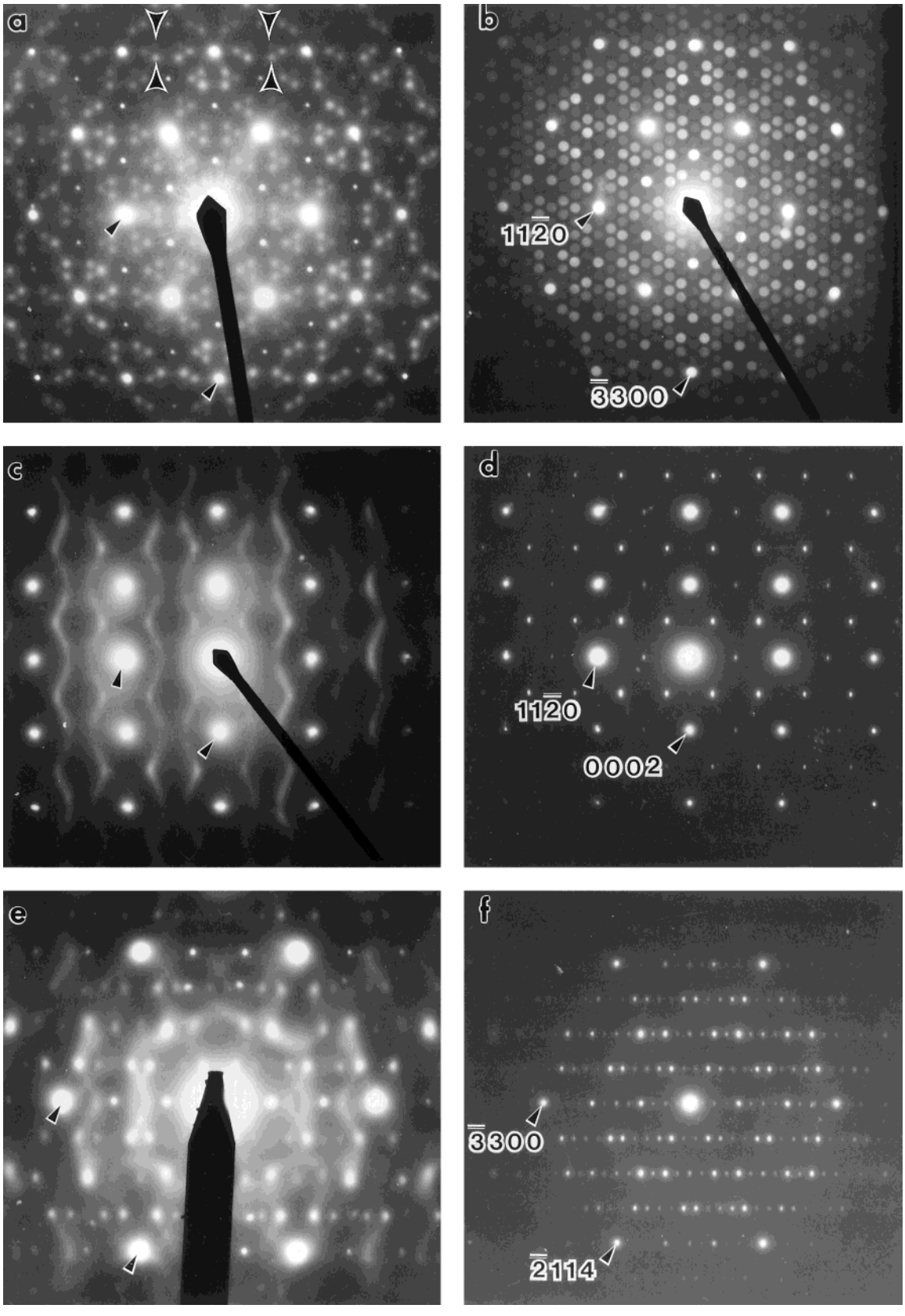

FIG. 2. (a) [001], (c) [$\bar{1}$10], and (e) [441] zone axis electron diffraction patterns typical of the ''disordered'' phases of both $Co_{2+x}Sn_2$ and $Ni_{2+x}Sn_2$. (b, d, f) Corresponding diffraction patterns of the low-temperature, ordered superstructure phase. Indexing is with respect to the underlying $P6_3/mmc$ average structure.

Shape of the Diffuse Distribution

The diffuse distribution characteristic of the disordered phase has a complex three-dimensional shape that is difficult to describe in detail but would appear to be based on intertwined, undulating, approximately cylindrical channels of diffuse intensity running along the **c*** directions of reciprocal space. Only one of the two intertwined, undulating channels are visible in Fig. 2c as a result of the characteristic extinction condition described above. The presence of two intertwined, undulating channels, however, very quickly becomes apparent on rotation around **c*** (see, e.g., Figs. 3b and c). To get the approximate shape of the proposed channels, crystals were systematically tilted, keeping **c*** excited and marking where the diffuse distribution occurred as a function of rotation angle. The results were consistent with the notion of undulating, approximately cylindrical channels (centered on each average structure Bragg reflection) running along the **c*** directions of reciprocal space. The radius of these cylindrical channels at $l = 0$ is typically the largest ($\sim \frac{3}{8}|(\mathbf{a}^* + \mathbf{b}^*)|$ in Fig. 2c) and always decreases as l increases. This model of undulating, approximately cylindrical channels is also consistent with the diffuse distributions observed at more minor zone axis orientations such as the $[\bar{1}11]$ and $[\bar{1}\bar{1}1]$ zone axis diffraction patterns shown in Fig. 4.

Note the presence of clusters of three apparent superlattice reflections in Fig. 4a, as well as in Fig. 2a. The $[\bar{1}11]$ zone axis orientation, however, is rotated ~53.9° about the (**a*** + **b***) direction of reciprocal space with respect to the [001] orientation; i.e., the apparently localized superlattice reflections of Fig. 2a and Fig. 4a are in fact part of three interlocking, continuously extended (running on average along **c***), undulating lines of strong diffuse scattering (see Fig. 2c).

Diffuse Intensity Absences

The absence of diffuse intensity in the zero-order Laue zone (ZOLZ) at [110] zone axis orientations, i.e., in (110)* reciprocal lattice planes (see Fig. 3a) is also a characteristic feature (indeed an apparent characteristic extinction condition) of the ''disordered'' phase and is no accident, as is clear from a comparison of Figs. 3a and b; i.e., slight tilts away from the exact [110] zone axis orientation rapidly bring up diffuse intensity and show that significant diffuse intensity occurs just above and just below but not in the

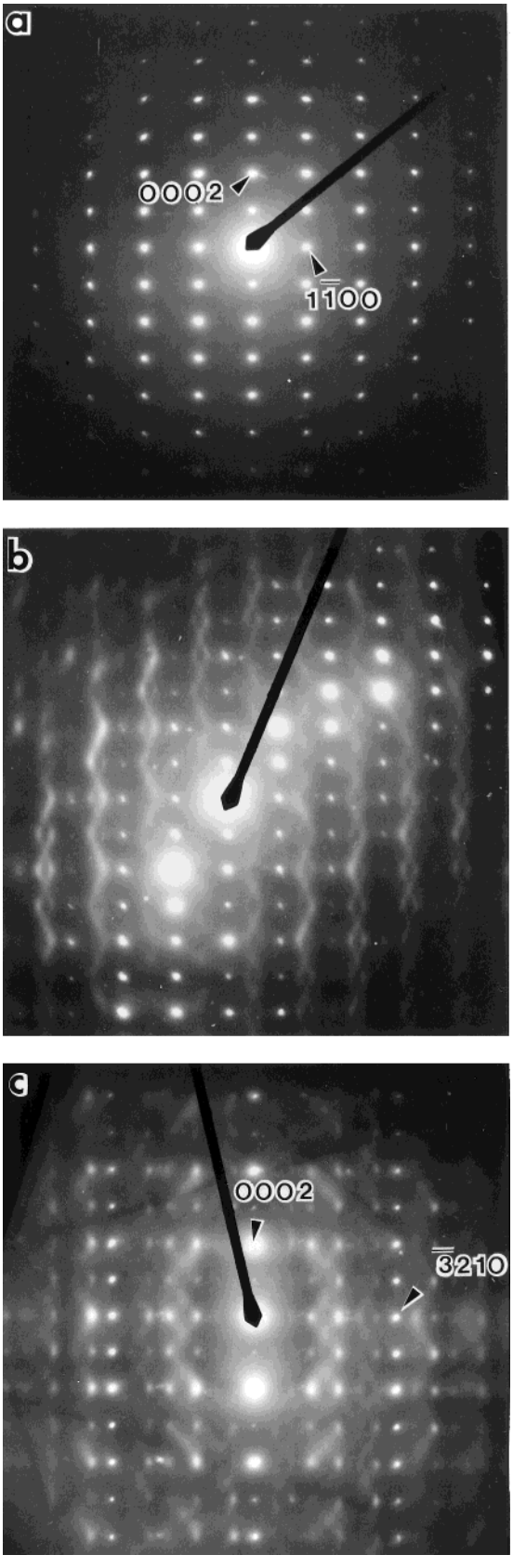

FIG. 3. (a) [110] and (c) [230] zone axis electron diffraction patterns typical of the ''disordered'' phases of $Co_{2+x}Sn_2$ and $Ni_{2+x}Sn_2$. (b) Taken tilted a few degrees away from [110]. Note the complete absence of diffuse intensity at the exact [110] zone axis orientation in (a) and the presence of two intertwined, undulating, approximately cylindrical channels of diffuse intensity running along the **c*** directions of reciprocal space in (b) and (c).

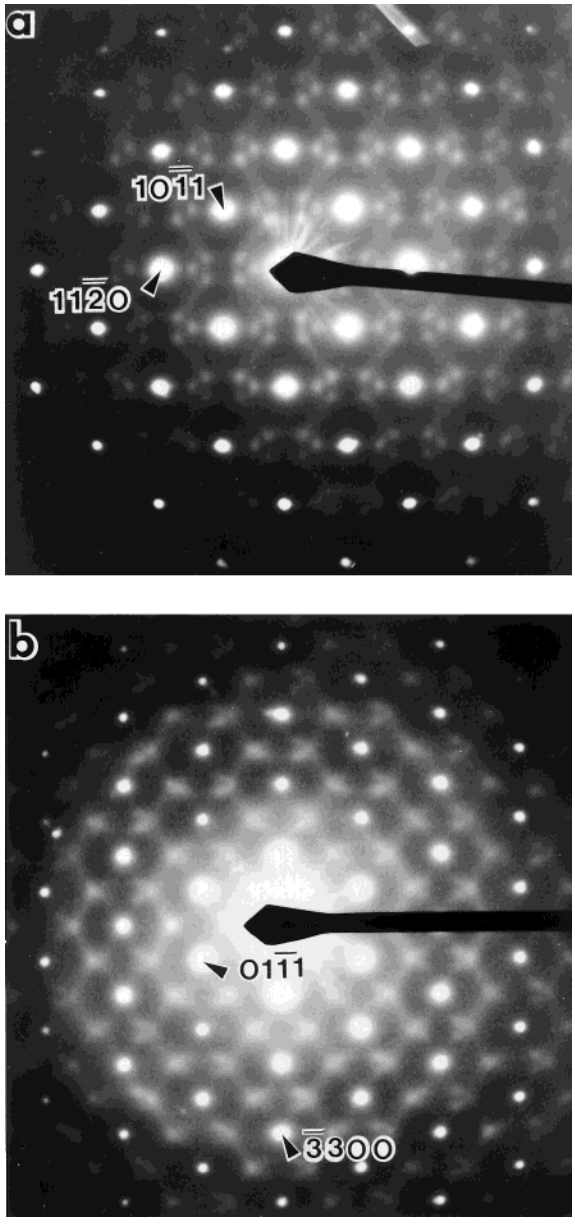

FIG. 4. (a) [$\bar{1}$11] and (b) [$\bar{1}\bar{1}$1] zone axis diffraction patterns typical of the ''disordered'' phases of $Co_{2+x}Sn_2$ and $Ni_{2+x}Sn_2$. Note the presence of clusters of three apparent superlattice reflections in (a) and the absence of diffuse scattering along $\mathbf{G} \pm h(\mathbf{a}^* - \mathbf{b}^*)$ directions of reciprocal space in (b).

(110)* reciprocal lattice plane itself. [Such a plane of diffuse intensity absence is strongly reminiscent of the planes of diffuse intensity absence, or so-called dark planes, characteristic of yttria cubic-stabilized zirconias (20, 21).] This absence of diffuse intensity in the (110)* reciprocal lattice planes also shows up in the absence of diffuse intensity along $\mathbf{G} \pm h(\mathbf{a}^* - \mathbf{b}^*)$ directions in Figs. 2a and 4b. A possible real space origin for this characteristic extinction condition is discussed below.

System and Composition-Dependent Features

A detailed system and composition-dependent study of the diffuse disribution was not the object of this paper. Nonetheless it is important to point out some features of the diffuse distributions that do change systematically with composition. While the general topology or shape of the diffuse distribution does not change significantly with composition, the absolute size does. Figure 5, for example, shows [$\bar{1}$10] zone axis SADPs of disordered $Ni_{2+x}Sn_2$ specimens for (a) $x = 0.68$, (b) $x = 1.05$, and (c) $x = 1.22$. Powder XRD patterns showed the specimens were homogeneous and gave unit cell dimensions in good agreement with those previously reported for the disordered $Ni_{2+x}Sn_2$ phase (6, 15). The characteristic sine wave-type diffuse streaking along the $\mathbf{c}^*$ direction of Fig. 2c is present in all three, but the amplitude associated with the sine wave clearly varies. The diffuse distribution passes through $\mathbf{G} \pm \varepsilon(\mathbf{a}^* + \mathbf{b}^*)$ regions of reciprocal space for $\mathbf{G} = h(\mathbf{a}^* + \mathbf{b}^*) + l\mathbf{c}^*$, l odd, with $\varepsilon = 0.21$, 0.25, and 0.28 for (a), (b), and (c) respectively. The parameter ε appears to be directly proportional to the composition as shown in Fig. 6.

4. INTERPRETATION

While a detailed interpretation of the observed diffraction data is beyond the scope of this paper, there are nonetheless important real space conclusions that can readily be drawn from the observed diffraction evidence. Thus, the characteristic absence of diffuse intensity in the ZOLZ at [110] zone axis orientations (see Fig. 3a) requires that there be the same number of occupied interstitial sites along each and every ⟨110⟩ string of close packed interstitial sites (see Fig. 1).

This can be deduced from a modulation wave approach to the observed diffuse distribution whereby the atomic scattering factor of the μth atom in the $\mathbf{T}$th unit cell is written as

$$f_\mu(\mathbf{T}) = f_\mu^{\text{av}} + \delta f_\mu(\mathbf{T}) \qquad [1]$$
$$= f_\mu^{\text{av}} \left(1 + \text{Re} \sum_{\mathbf{q}} a_\mu(\mathbf{q}) \exp(2\pi i \mathbf{q} \cdot \mathbf{T})\right).$$

Here μ labels the independent sites per average structure unit cell, $\mathbf{T}$ the position of the particular unit cell, f_μ^{av} the atomic scattering factor of the μth site in the average structure, and $\mathbf{T} + \mathbf{r}_\mu$ the position of the μth site in the average structure [see Refs. (16, 22–24)]. Note that $a_\mu(-\mathbf{q}) = a_\mu(\mathbf{q})^*$ and that the summation over $\mathbf{q}$ is understood to range over the whole of the first Brillouin zone of the average structure. Any arbitrary ordering scheme can thereby be described. The observed highly structured diffuse distribution shows which wavevectors need to be included in the

summation over **q**. Such a modulation wave approach has been successfully used on several previous occasions (9, 22, 23) to synthesize real space ordering patterns compatible with observed diffraction data. [Note that each compositional modulation wave will of necessity also be accompanied by a displacive modulation wave

$$\mathbf{u}_\mu(\mathbf{T}) = \mathrm{Re} \sum_{\mathbf{q}} \mathbf{e}_\mu(\mathbf{q}) \exp(2\pi i \mathbf{q} \cdot \mathbf{T}) \qquad [2]$$

characterized by the same modulation wavevector and corresponding to the structural relaxation associated with the distribution of interstitial ions. Again, the summation over **q** is understood to range over the whole of the first Brillouin zone of the average structure and $\mathbf{e}_\mu(-\mathbf{q}) = \mathbf{e}_\mu(\mathbf{q})^*$.] The absence of diffuse intensity in (110)* reciprocal lattice planes implies that $a_\mu(\mathbf{q}) = 0$ for any modulation wavevector in the (110)* reciprocal lattice plane, i.e., for any modulation wavevector exactly perpendicular to the [110] directions of real space. Hence the average occupancy of interstitial sites along each and every ⟨110⟩ string must be the same as the crystal average, i.e., f_μ^{av}.

Why must the average occupancy along such ⟨110⟩ strings be the same? Consider the effect of strain in such systems (see Fig. 7). Every time a particular interstitial site is occupied, the five surrounding Sn atoms are repelled (the three Sn atoms in the same plane as the interstital along the three ⟨1$\bar{1}$0⟩ directions and the two Sn atoms directly above and below the interstital along [001]), whereas the six surrounding *M* ions are attracted (along the three ⟨1$\bar{1}$0⟩ directions) toward the interstitial site. The effect is that the Sn sublattice is locally expanded along the three close-packed ⟨110⟩ directions, while the *M* sublattice is locally contracted. The reverse happens relative to the average if a particular site is vacant. An increase above the average of the number of occupied interstitial sites in any particular ⟨110⟩ string of potential interstitial sites would therefore necessarily imply macroscopic strain and hence does not occur. (Note that in the case of η'-Cu_6Sn_5 (4), it has recently been shown that the magnitude of the corresponding relaxational shifts surrounding an interstitial Cu ion are ~0.2, 0.15, and 0.1 Å, respectively. The direction and magnitude of these relaxations in the case of η'-Cu_6Sn_5 are likely to be similar in the case of $Ni_{2+x}Sn_2$ and $Co_{2+x}Sn_2$. They are certainly consistent with the known crystal structures of Ni_3Sn_2 and Co_3Sn_2 [see, e.g., Fig. 2 of (6)]).

Minimization of strain suggests the importance of

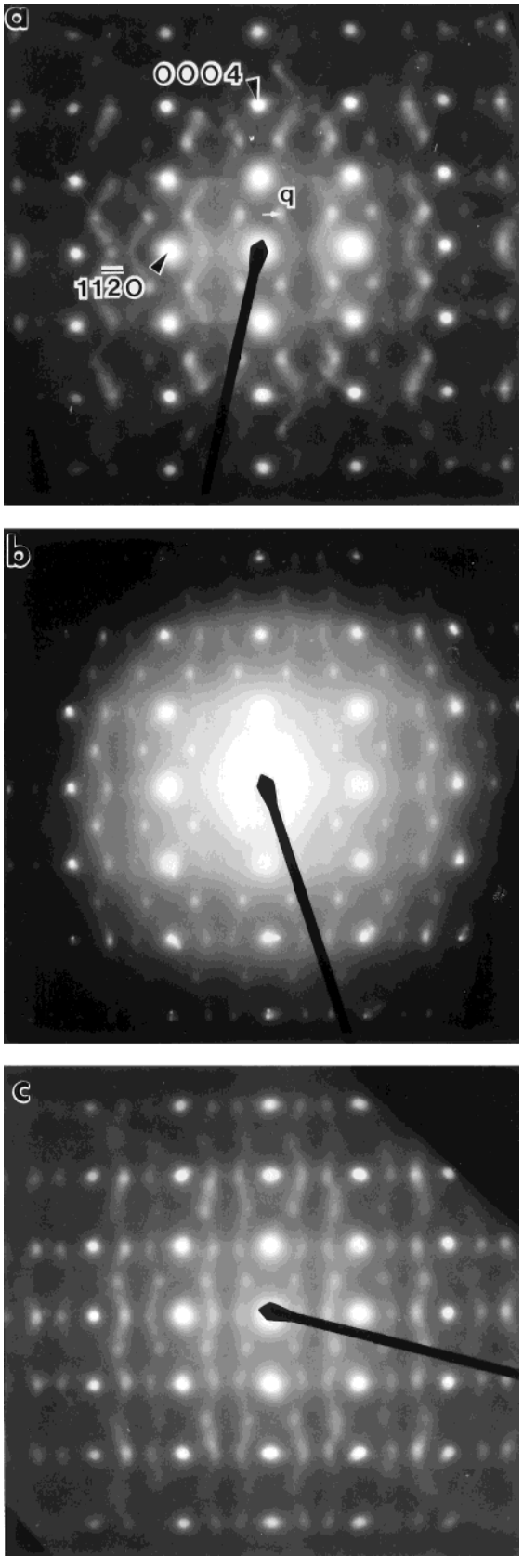

FIG. 5. [$\bar{1}$10] zone axis diffraction patterns of disordered $Ni_{2+x}Sn_2$ specimens for (a) $x = 0.68$, (b) $x = 1.05$, and (c) $x = 1.22$. The diffuse distributions pass through $\mathbf{G} \pm \varepsilon(\mathbf{a}^* + \mathbf{b}^*)$ regions of reciprocal space for $\mathbf{G} = h(\mathbf{a}^* + \mathbf{b}^*) + l\mathbf{c}^*$, l odd. Note the strong composition dependence of the parameter ε.

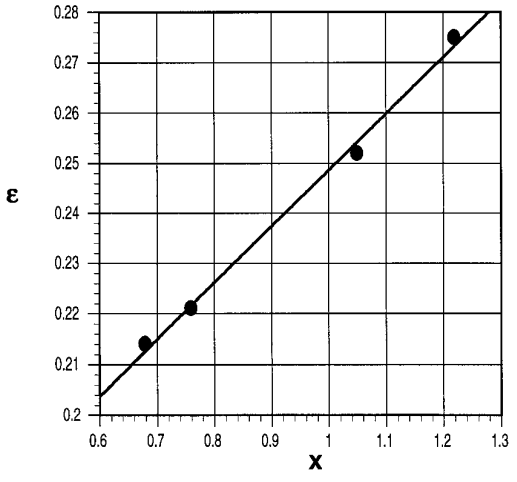

FIG. 6. Measured relationship between the parameter ε (see Fig. 5) and composition x for the $Ni_{2+x}Sn_2$ system.

avoiding too many occupied interstitial sites in a row along the close-packed ⟨110⟩ directions (see Fig. 1) and undoubtedly plays an important role in determining the allowed modulation wavevectors and hence the observed diffuse distribution.

Direct diffraction evidence that lattice relaxations surrounding the occupied interstitial sites do indeed occur along the three $\langle 1\bar{1}0\rangle$ real space directions corresponding to the "first-order size effect" described by Welberry (19) can be obtained from the very clear "size effect" transfer

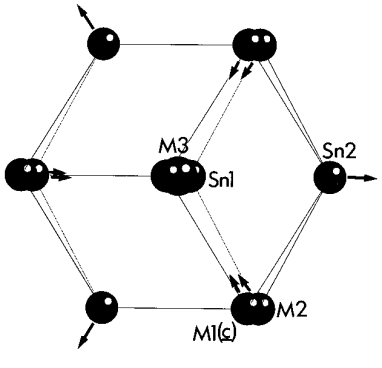

FIG. 7. Eleven-coordinate Edshammar polyhedron of Sn1, Sn2, $M1$, and $M2$ atoms coordinating an occupied $M3$ interstitial site (the same interstitial site that is visible within the unit cell of Fig. 1) and the associated structural relaxations away from average lattice positions. The unit cell orientation is the same as that shown in Fig. 1. The three surrounding Sn2-type atoms are repelled along the three $\langle 1\bar{1}0\rangle$ directions and the two Sn1 atoms directly above and below the interstital along [001], whereas the six surrounding $M1$ and $M2$ ions are attracted (along the three $\langle 1\bar{1}0\rangle$ directions) toward the interstital site. The effect is that the Sn sublattice is locally expanded along the three close-packed ⟨110⟩ directions, whereas the M sublattice is locally contracted along the three close-packed ⟨110⟩ directions.

of intensity from the high- to the low-angle side of the $(h\mathbf{a}^* + k\mathbf{b}^*) \cdot \frac{1}{3}[-\mathbf{a} + \mathbf{b}] = \frac{1}{3}(-h + k) =$ an integer lines of reciprocal space in Fig. 2a. As shown in (24), the "size effect" contribution to the observed diffuse intensity distribution is given by

$$I_4(\mathbf{G} + \mathbf{q}) = N^2 \mathrm{Re} \sum_{\mu} \sum_{\mu'} f_{\mu}^{\mathrm{av}} f_{\mu'}^{\mathrm{av}*} \exp(-2\pi i[\mathbf{G} + \mathbf{q}] \cdot [r_{\mu} - r_{\mu'}]) \times 2\pi a_{\mu}(\mathbf{q})([\mathbf{G} + \mathbf{q}] \cdot \mathbf{e}_{\mu'}(\mathbf{q})^* \exp(i\pi/2). \quad [3]$$

From a modulation wave point of view, there are six distinct atom sites per parent unit cell: $M1$ at 000, $M2$ at $00\frac{1}{2}$, $M3$ at $\frac{1}{3}, \frac{2}{3}, \frac{3}{4}$, $M4$ at $\frac{2}{3}, \frac{1}{3}, \frac{1}{4}$, Sn1 at $\frac{1}{3}, \frac{2}{3}, \frac{1}{4}$, and Sn2 at $\frac{2}{3}, \frac{1}{3}, \frac{3}{4}$ (see Figs. 1 and 7). Occupational ordering and hence nonzero $a_{\mu}(\mathbf{q})$ values can be associated with only two of these, namely, $M3$ and $M4$, the two interstitial sites per parent unit cell.

To evaluate the above expression it is necessary to correlate the displacive modulation wave amplitudes with the corresponding compositional modulation wave amplitudes. Consider, for example, the $\mu = M3, \mu' =$ Sn2 contribution to the above expression (see Fig. 7). In the "first-order size effect" described by Welberry (19) each atom is allowed to shift from its mean lattice site to alleviate the size effect strain with its nearest neighbors only. In modulated structure language this is equivalent to the statement that

$$\mathbf{u}_{\mathrm{Sn2}}(\mathbf{T}) \propto (\mathbf{a} - \mathbf{b})\delta f_{\mathrm{M3}}(\mathbf{T}) + (-2\mathbf{a} - \mathbf{b})\delta f_{\mathrm{M3}}(\mathbf{T} + \mathbf{a}) + (\mathbf{a} + 2\mathbf{b})\delta f_{\mathrm{M3}}(\mathbf{T} - \mathbf{b}), \quad [4]$$

which in turn implies that

$$\mathbf{e}_{\mathrm{Sn2}}(\mathbf{q}) \propto a_{\mathrm{M3}}(\mathbf{q})\{1 \cdot (\mathbf{a} - \mathbf{b}) + \exp(2\pi i\mathbf{q} \cdot \mathbf{a}) \cdot (-2\mathbf{a} - \mathbf{b}) + \exp(-2\pi i\mathbf{q} \cdot \mathbf{b}) \cdot (\mathbf{a} + 2\mathbf{b})\}. \quad [5]$$

The corresponding contribution to $I_4(\mathbf{G} + \mathbf{q})$ is then proportional to

$$-2\pi N^2 f_{\mathrm{M4}}^{\mathrm{av}} f_{\mathrm{Sn}} \{(\mathbf{G} + \mathbf{q}) \cdot (-\mathbf{a} + \mathbf{b}) \sin(2\pi[\mathbf{G} + \mathbf{q}] \cdot \tfrac{1}{3}[-\mathbf{a} + \mathbf{b}]) + (\mathbf{G} + \mathbf{q}) \cdot (2\mathbf{a} + \mathbf{b}) \sin(2\pi[\mathbf{G} + \mathbf{q}] \cdot \tfrac{1}{3}[2\mathbf{a} + \mathbf{b}]) + (\mathbf{G} + \mathbf{q}) \cdot (-\mathbf{a} - 2\mathbf{b}) \sin(2\pi[\mathbf{G} + \mathbf{q}] \cdot \tfrac{1}{3}[-\mathbf{a} - 2\mathbf{b}])\} \quad [6]$$

and clearly has the correct functional form to explain the "size effect" transfer of intensity from the high- to the low-angle side of the $(h\mathbf{a}^* + k\mathbf{b}^*) \cdot \frac{1}{3}[-\mathbf{a} + \mathbf{b}] = \frac{1}{3}$

$(-h + k)$ = an integer lines of reciprocal space in Fig. 2a. (Note that the $\mu = M4$, $\mu' =$ Sn1 contribution is identical, whereas the $\mu = M3$, $\mu' = M1$ and $M2$ as well as $\mu = M4$, $\mu' = M1$ and $M2$ terms have the same functional form but with opposite sign as is to be expected given that an occupied interstitial site attracts rather than repels neighboring $M1$ and $M2$ ions.)

A further important real space conclusion can be drawn from the observation that the characteristic sine wave-type diffuse streaking along the **c*** direction of Fig. 2c passes through $\mathbf{G} \pm \frac{1}{4}(\mathbf{a}^* + \mathbf{b}^*)$ regions of reciprocal space only for $\mathbf{G} = h(\mathbf{a}^* + \mathbf{b}^*) + l\mathbf{c}^*$, l odd, whereas it passes through $\mathbf{G} \pm \frac{3}{8}(\mathbf{a}^* + \mathbf{b}^*)$ regions of reciprocal space for $\mathbf{G} = h(\mathbf{a}^* + \mathbf{b}^*) + l\mathbf{c}^*$, l even. In terms of the language of modulated structures (8, 23) this observation requires that the corresponding compositional eigenvectors $a(\mathbf{q}) = (a_{M3}, a_{M4})$ take the form $(a, -a)$ for $\mathbf{q} = \frac{1}{4}(\mathbf{a}^* + \mathbf{b}^*)$ and (a, a) for $\mathbf{q} \sim \frac{3}{8}(\mathbf{a}^* + \mathbf{b}^*)$. The former eigenvector implies that if a particular $M3$ interstitial site is occupied, then its c glide-related $M4$ site (see Fig. 1) will tend to be vacant, whereas the latter eigenvector implies that if a particular $M3$ intersititial site is occupied, then its c glide-relate $M4$ site will also tend to be occupied. The observed sine wave-type diffuse streaking along the **c*** direction of Fig. 2c shows that the allowed value of ε for a particular value of l [for compositional modulation waves of wavevector $\mathbf{q} = \varepsilon(\mathbf{a}^* + \mathbf{b}^*) + l\mathbf{c}^*$] is bivalued and dependent on whether the eigenvector is of $(a, -a)$ or (a, a) type. Clearly, ordering correlations between the $M3$ and $M4$ sublattices are very important for this system.

The importance of strain minimization suggests the relevance of the cluster expansion approach to short-range order as set out in (11–14). The equations developed therein are not, however, in their current form, directly applicable to the present case as a result of the fact that correlated ordering clearly occurs on sublattices not separated by Bravais lattice vectors, i.e., on the $M3$ and $M4$ sublattices. The basic idea, however, that the localization of the diffuse distribution may arise from a requirement that atomic clusters of specific polyhedral types should all satisfy as far as is possible a particular cluster relation—usually that the cluster should have the macroscopic composition—is most probably also relevant here. The obvious candidates for such clusters are the nearest-neighbor tetrahedral and octahedral polyhedra in the approximately hcp lattice formd by the $M3$ and $M4$ sublattices.

A requirement that each such polyhedron (see Fig. 1) should have the macroscopic composition (e.g., for $x = 1$, two occupied and two unoccupied sites for each of the four Bravais lattice independent tetrahedra per average structure unit cell and three occupied and three unoccupied sites for each of the two Bravais lattice independent octahedra per average structure unit cell) exactly does not, however, in this case lead to a continuous diffuse distribution but rather to the only observed superstructure phase corresponding to $\mathbf{q} = \frac{1}{4}(\mathbf{a}^* + \mathbf{b}^*)$ and with $a_{M4} = -a_{M3}$. For values of **q** other than $\frac{1}{4}(\mathbf{a}^* + \mathbf{b}^*)$, however, it appears not to be possible to satisfy the above constraints exactly.

It may be possible to generalize the cluster expansion approach as set out in (11–14) to encompass the current system and hence to obtain more insight into the nature of the short-range order responsible for the observed diffuse distribution. Further work along these lines is in progress. Other potential approaches include Monte Carlo simulation based on appropriate local ordering rules [see, e.g., (24)] or computer simulation of a distribution of intersitial ions compatible with the observed diffuse distribution based on a modulation wave approach [see, e.g., (9)]. Such approaches, however, are beyond the scope of this paper.

REFERENCES

1. A. Kjekshus and W. B. Pearson, *Prog. Solid State Chem.* **1,** 83 (1964).
2. P. Villars and L. D. Calvert (Eds.), "Pearsons Handbook of Crystallographic Data for Intermetallic Phases." ASM, Cleveland, OH, 1992.
3. M. Hansen, (Ed.), "Constitution of the Binary Alloys." McGraw-Hill, New York, 1958.
4. A-K. Larsson, L. Stenberg, and S. Lidin, *Acta Crystallogr. B* **50,** 636 (1994).
5. S. Lidin and A-K. Larsson, *J. Solid State Chem.* **118,** 313 (1995).
6. H. Fjellvåg and A. Kjekshus, *Acta Chem. Scand. A* **40,** 23 (1986).
7. A-K. Larsson, L. Stenberg, and S. Lidin, *Acta Chem. Scand.* **49,** 800 (1995).
8. R. L. Withers, T. R. Welberry, J. G. Thompson, and J. D. Fitz Gerald, *in* "Methods of Structural Analysis of Modulated Structures and Quasicrystals" (J. M. Perez-Mato, F. J. Zuniga, and G. Madariaga, Eds.), p. 443. World Scientific, Singapore, 1991.
9. T. R. Welberry, R. L. Withers, and S. C. Mayo, *J. Solid State Chem.* **115,** 43 (1995).
10. R. L. Withers, J. G. Thompson, Y. Xiao, and R. J. Kirkpatrick, *Phys. Chem. Min.* **21,** 421 (1994).
11. M. Sauvage and E. Parthé, *Acta Crystallogr. A* **30,** 239 (1974).
12. R. de Ridder, G. van Tendeloo, and S. Amelinckx, *Acta Crystallogr. A* **32,** 216 (1976).
13. R. de Ridder, D. van Dyck, G. van Tendeloo, and S. Amelinckx, *Phys. Status Solidi A* **40,** 669 (1977).
14. D. van Dyck, R. de Ridder, and S. Amelinckx, *Phys. Status Solidi A* **59,** 513 (1980).
15. M. Ellner, *J. Less-Common Met.* **48,** 21 (1976).
16. J. M. Perez-Mato, G. Madariaga, F. J. Zuniga, and S. A. Garcia Arribas, *Acta Crystallogr. A* **43,** 216 (1987).
17. P. Brand, *Z. Anorg. Allg. Chem.* **353,** 270 (1967).
18. H. Rajeswari and H. Manihar, *Indian J. Pure Appl. Phys.* **8,** 363 (1970).
19. T. R. Welberry, *J. Appl. Crystallogr.* **19,** 382 (1986).
20. T. R. Welberry, R. L. Withers, J. G. Thompson, and B. D. Butler, *J. Solid State Chem.* **100,** 71 (1992).
21. T. R. Welberry, B. D. Butler, J. G. Thompson, and R. L. Withers, *J. Solid State Chem.* **106,** 461 (1993).
22. T. R. Welberry and R. L. Withers, *J. Appl. Crystallogr.* **23,** 303 (1990).
23. T. R. Welberry, R. L. Withers, and J. C. Osborn, *Acta Crystallogr. B* **46,** 267 (1990).
24. B. D. Butler, R. L. Withers, and T. R. Welberry, *Acta Crystallogr. A* **48,** 737 (1992).
25. S. Matsumura, K. Takano, N. Kuwano, and K. Oki, *J. Cryst. Growth* **115,** 194 (1991).